DESY 94-191
MPI-PhE/94-23
October 1994

ISSN 0418-9833

NEW EXPERIMENTAL RESULTS AT HERA [1]

M. Kuhlen
Max-Planck-Institut für Physik
Werner-Heisenberg-Institut
Föhringer Ring 6
D-80805 München
Germany
E-mail: h1kmku@dsyibm.desy.de

representing the H1 and ZEUS Collaborations

Abstract

Recent measurements by the ZEUS and H1 collaborations of the hadronic final state in deep inelastic scattering at HERA are reviewed. QCD is studied by means of charged particle spectra, jet rates and inclusive energy flows.

[1] talk given at the VIth Rencontre de Blois, "Au Cœur de la Matière", Blois, June 1994

1 Introduction

HERA has opened a new kinematic domain to study QCD in deep inelastic scattering (DIS), $ep \to e +$ hadrons (Fig. 1). Measurements of the hadronic final state will be presented here, while the complementary measurements of the cross section in terms of the proton structure function F_2 are discussed in [1]. Diffractive processes have emerged as a field in their own right and are covered by [1] and [2].

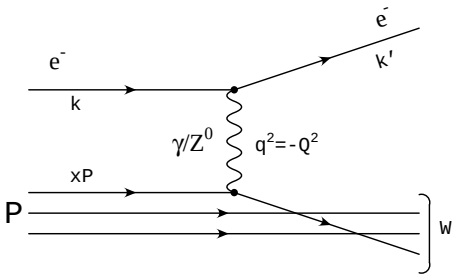

Figure 1: Feynman graph for deep inelastic scattering.

In the simple quark parton model of DIS, a quark is scattered out of the proton by the virtual boson emitted from the scattering lepton. QCD modifies this naive picture. Gluons may be radiated before (initial state radiation) and after (final state radiation) the boson-quark vertex, and the boson may also interact with a gluon inside the proton by means of a quark line (boson-gluon fusion) (Fig. 2). QCD radiation in the final state is equivalent to the situation in e^+e^-annihilation, while initial state QCD radiation is unique to DIS. It can be viewed as the materialization of quantum fluctuations inside the proton, when it is probed by a boson in the measuring process. The partonic structure of the proton thus becomes observable in the hadronic final state. Of particular interest is the kinematic regime at small Bjorken x, not accessible at pre-HERA DIS experiments, where novel QCD dynamics are expected to play a rôle.

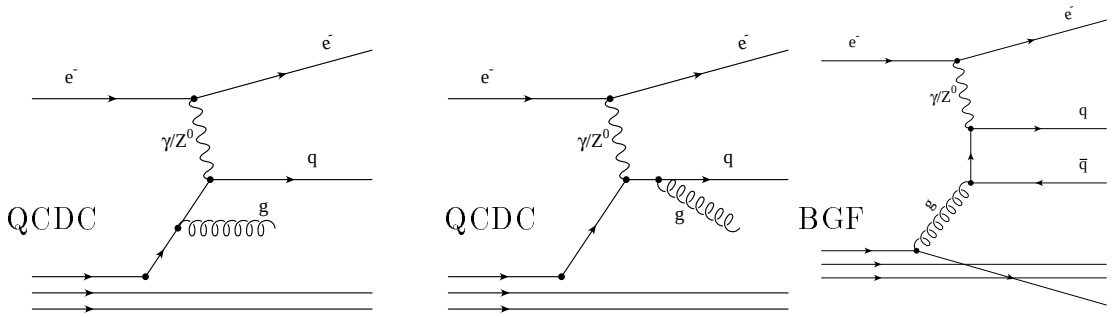

Figure 2: Diagrams for DIS in first order QCD: QCD Compton (QCDC) and boson-gluon fusion (BGF) processes.

The HERA results presented in this report follow a route from the "current" region, much explored in e^+e^-annihilation, towards the relatively "unknown" of the initial state cascade at small x. "Current" refers to the region which can be associated with the scattered quark in the quark parton model, as opposed to the target fragmentation region of the proton remnant, and an intermediate regime. Hence charged particle spectra for the current region are measured and compared with data from e^+e^-annihilation. The measurement of the QCD Compton and boson-gluon fusion processes (Fig. 2) via jet rates allows the determination of the strong coupling constant α_s and the gluonic structure of the proton. The measurement of energy flows

leads furthest into the regime of small x and away from the current jet, where first signs of novel QCD dynamics may become visible. This could be the transition from the conventional Altarelli-Parisi [3] parton evolution to the proposed Lipatov type of evolution [4].

In 1992 and 1993, HERA collided electrons of $E_e = 26.7$ GeV with protons of $E_p = 820$ GeV, resulting in a centre of mass energy of $\sqrt{s} = 296$ GeV. The kinematic region covered with the present data is roughly $10^{-4} < x < 10^{-1}$, $10 < Q^2 < 1000$ GeV ^{2} and W about 40-300 GeV, where W is the invariant mass of the hadronic system, Q^2 the negative 4-momentum transfer squared, and x the Bjorken scaling variable, to be identified with the proton momentum fraction carried by the scattering parton in the quark parton model. HERA thus covers a large kinematic range available to study the evolution of observables; to give just one example, the running of the strong coupling constant α_s can be measured for Q^2 values over 2 orders of magnitude.

The two detectors [5] operated at HERA, ZEUS and H1, are large multipurpose "4π" detectors built around the beam line (example in Fig. 3). Inner tracking detectors for charged particle detection are surrounded by a magnet and calorimetry. Both, the scattered electron, serving as a tag for DIS events, and the hadronic final state are measured. The determination of the event kinematics by these two measurements is overconstrained, and allows to make use of both informations in an optimal way, depending on the analysis goals [6].

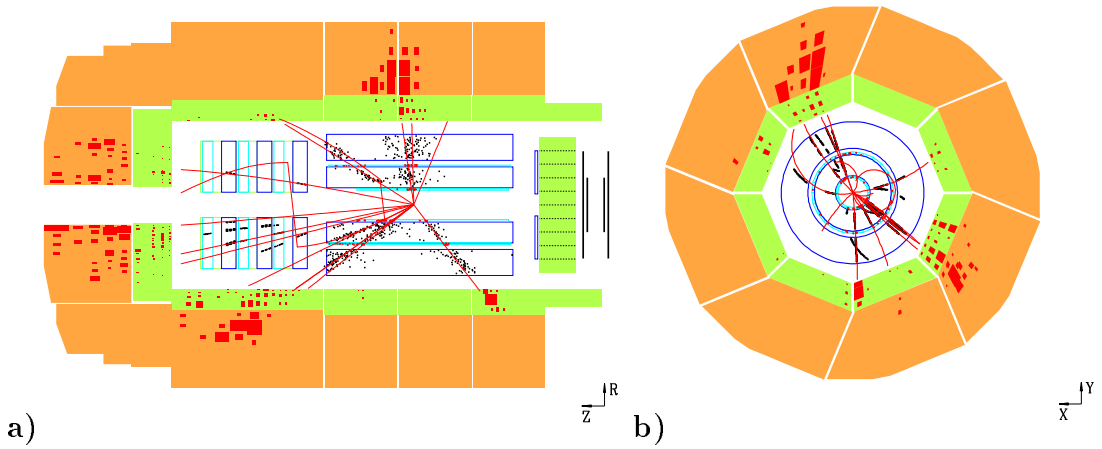

Figure 3: A DIS event with the scattered electron and two well separated jets detected in the H1 detector. The proton remnant leaves mostly undetected in $+z$ direction. Shown are cuts **a)** parallel and **b)** perpendicular to the beam line.

Among the analyses presented here, the ones from the 1992 run, corresponding to about 25 nb^{-1} of data accumulated by each of the two experiments ZEUS and H1, are already published, while the ones from the 1993 run, which yielded 300-500 nb^{-1} per experiment, are still preliminary. From the 1994 run some 2000 nb^{-1} are expected.

2 QCD Models

In order to correct the data for detector effects and also to estimate the influence of non-perturbative hadronization effects on perturbative observables, Monte Carlo methods are utilized. A generator based on a model of the underlying physics produces event by event a set of final state particles, which are then fed into a program simulating the detector response. The various generators employ different ways of generating QCD emissions: first order QCD matrix elements, or parton showers to all orders in the leading logarithmic approximation (modelled

either as bremsstrahlung-like cascades or as emissions from colour dipoles), or a combination of the two. By comparing the data to various models incorporating different approximations of the relevant QCD processes, insight into the underlying physics can be gained. The naive quark parton model (QPM) without any gluon radiation, in which hadrons are produced from fragmentation of the string between the current quark and the remnant di-quark, is also used for illustration.

The model abbreviated as MEPS [7] incorporates the QCD matrix elements up to first order (Fig. 2), with additional soft emissions generated by adding leading log parton showers. Two different pure parton shower models are used, referred to as PSWQ [7] and HERWIG [8]. Both are based on leading log parton showers, but they differ in their way of emulating QCD coherence effects. In the colour dipole model CDM [9], gluons are emitted from a chain of independently radiating dipoles which are spanned by colour connected partons. Since all radiation is assumed to stem from the dipole formed by the struck quark and the remnant, boson-gluon fusion events cannot be generated in this way; they are instead taken from the QCD matrix elements.

3 Charged Particle Spectra

Basic properties of the hadronic final state in terms of charged particle production have been studied by ZEUS and H1. Rather than in the HERA laboratory frame, they are studied in either the hadronic centre of mass system (CMS) or in the Breit system as more natural frames of reference, eliminating the artificial transverse boost due to the scattered lepton.

The CMS is defined as the centre of mass system of the incoming proton and the virtual boson, i.e. the centre of mass system of the hadronic final state with invariant mass W . The z-axis is defined by the direction of the virtual boson. In the QPM, the scattered current quark and the proton remnant are back to back, parallel to the virtual boson direction, each with momentum $W/2$. The current region is therefore conventionally defined by all particles with longitudinal momentum $p_z > 0$.

The Breit system is connected with the CMS by a longitudinal boost along the virtual boson direction. It is defined by the condition that the virtual boson does not transfer energy, only momentum. In the QPM, the scattering quark just reverses its momentum of magnitude $Q/2$. In contrast to the CMS, the proton remnant is a mere spectator and does not change momentum. Again, particles with $p_z > 0$ are assigned to the current region [2].

Charged particle spectra from H1 [10] in the hadronic CMS for longitudinal (p_z) and transverse (p_T) momentum components with respect to the virtual boson direction are shown in Fig. 4 for an average W of 117 GeV .

The scaled longitudinal momentum spectrum of x_F , where the particle momenta are divided by the maximal possible momentum, $x_F = 2p_z/W$, is a steeply falling distribution, only in very rough agreement with previous DIS data from μN scattering at much lower W , $\langle W \rangle = 14$ GeV [11]. The H1 distribution is somewhat steeper, an indication for QCD induced scaling violations. The proliferation of particles at small x_F is due to the increase of phase space for the fragmentation process with increasing W : starting with a larger energy of the primary quark, more particles can be produced in the fragmentation chain until there is not enough energy left for producing a pion. Data from a different reaction, e^+e^- annihilation at LEP with similar W ($W^2 = Q^2 = s$ for e^+e^-), are also compared to the H1 data. The DELPHI

[2] Obviously, the definition of a current region depends on the frame of reference and has no absolute meaning; one is free to choose the frame which is best suited for the physics issue to be displayed.

data [12], divided by two to account for the two jets in e^+e^-annihilation, agree well with the H1 data for $x_F > 0.15$. At smaller x_F , the H1 data lie significantly below the LEP data.

At HERA, contributions to the transverse momenta of particles from intrinsic p_T in the proton and from fragmentation are expected to be small, leaving gluon radiation as the dominating source. As a sensitive measure of this effect the so-called seagull plot is presented in Fig. 4b, which gives the average transverse momentum squared, $\langle p_T^2 \rangle$, as a function of x_F. With increasing x_F, the average transverse momentum squared increases by about an order of magnitude. Comparing the H1 data at $\langle W \rangle = 117$ GeV to EMC data [11] at $\langle W \rangle = 14$ GeV , much larger transverse momenta are observed. This increase has to be attributed to increased QCD radiation. A scenario without QCD radiation, the QPM, gives a factor of about 5-10 less $\langle p_T^2 \rangle$. As to the strength of this effect, the models differ in their predictions. MEPS and CDM describe the data adequately, while PSWQ is only marginally compatible with the data. HERWIG differs significantly from the data, not only in magnitude, but also in the shape of the spectrum.

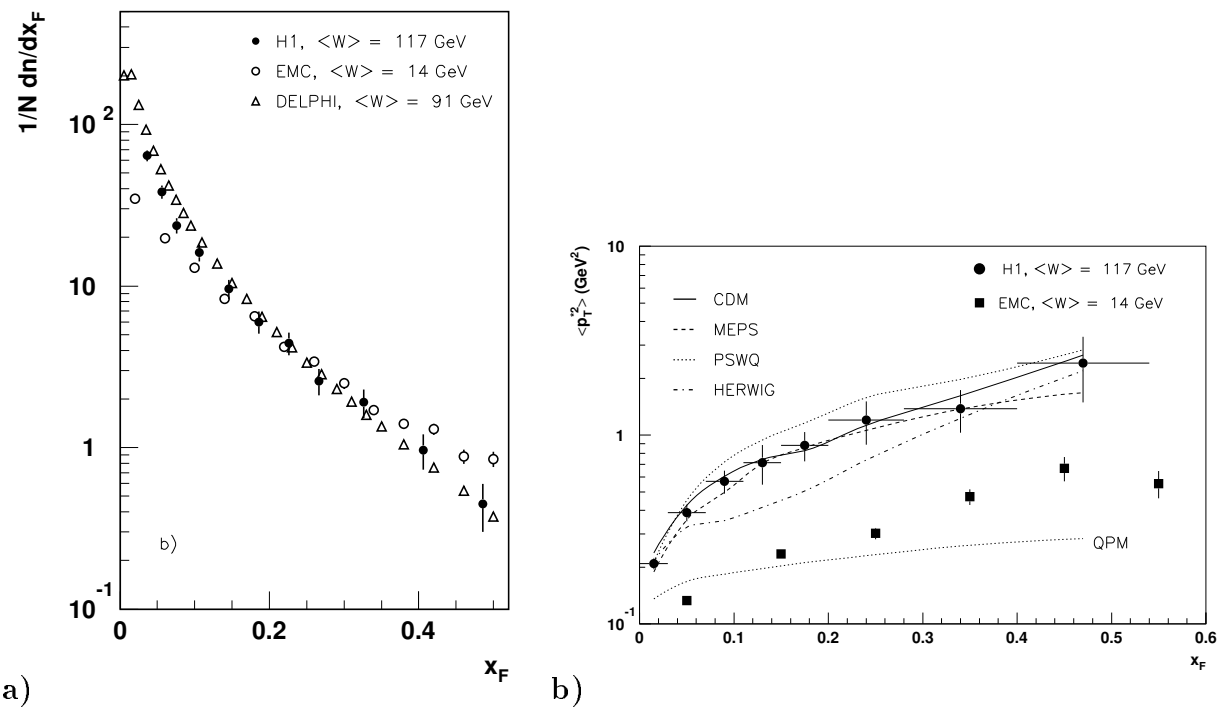

Figure 4: **a)** Scaled charged particle spectrum ($x_F = 2p_z/W$) in the CMS from H1, normalized to the number of events N, with n refering to the number of particles. The H1 data are compared with data from EMC and DELPHI. **b)** Seagull plot from H1: $\langle p_T^2 \rangle$ as a function of x_F for charged particles in the CMS, compared to different model predictions and EMC data.

ZEUS data on charged particle multiplicities and momenta are obtained in the Breit current region. In order to have good acceptance in the current region, a cut $x > 1.6 \cdot 10^{-4}$ was chosen. As the current quark has momentum $Q/2$, Q is the natural scaling variable in the Breit system. In Fig. 5a the mean charged multiplicity $n_{\rm ch}$ in the current region (multiplied by two) can be seen to rise with Q^2 , a consequence of the increase of phase space available for fragmentation. The slope agrees very well with the one observed in e^+e^-annihilation at PETRA and LEP [13].

Not just the mean, also the shape of the multiplicity distribution is of interest. It is presented in Fig. 5b in the form of the so-called KNO plot [14]. The distribution of events is plotted in the variable $z = n_{\rm ch} / \langle n_{\rm ch} \rangle$, i.e. the multiplicity normalized to the average multiplicity. These distributions are multiplied by $\langle n_{\rm ch} \rangle$ in the plot in order to compare

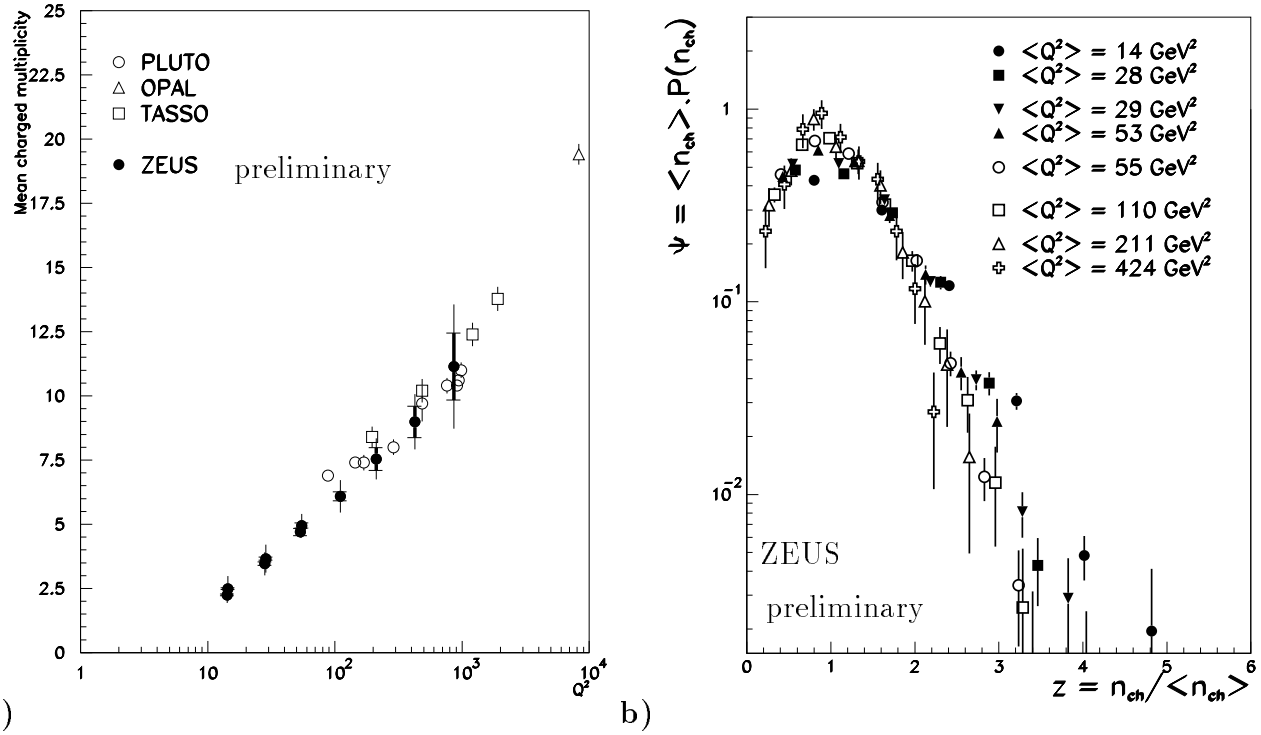

Figure 5: **a)** Mean charged multiplicity in the Breit current region from ZEUS as a function of Q^2 . The ZEUS data are scaled by a factor 2. The fat error bars are statistical errors, the thin ones statistical and systematic errors added in quadrature. Also shown are e^+e^-data from PETRA and LEP. **b)** The KNO plot for ZEUS data at different values of Q^2 . Shown are statistical errors only.

distributions from different kinematic regions. The ZEUS spectra for the KNO variable are approximately independent of Q^2 for a wide range of different Q^2 values from 14 to 400 GeV^2 .

The momentum spectra for charged particles in the Breit current region (see Fig. 6) are given in the scaled variable $x_p = 2p/Q$, i.e. the momenta are scaled with the momentum of the current quark. Rather than plotting x_p directly, $\ln(1/x_p)$ is used in order to enhance the soft part of the spectrum (to the right side). Up to a normalization factor, the shapes of these "hump backed" distributions have been calculated [15] using the modified leading log approximation (MLLA) [16] of QCD. They are calculated for partons, but can be compared to data under the assumption of local parton hadron duality (LPHD) [17], i.e. the hypothesis that the properties of the partonic final state are reflected in the hadronic final state up to a normalization constant. For the ZEUS data the peak of the hump backed distribution moves towards the soft region with increasing Q^2 , in qualitative agreement with the calculation [15]. In Fig. 6b the peak positions of the hump are plotted as a function of Q and are seen to line up quite nicely with data from e^+e^-annihilation [18]. The slope is smaller than what would be expected from a mere phase space model of hadronization - a hint for the presence of soft colour coherence, i.e. destructive interference of successive gluon emission [15]. However, it has been argued that such an effect can also be obtained in the Lund string fragmentation without explicit coherence effects [19].

4 Jet Physics: α_s and the Gluon Content of the Proton

Hard gluon radiation at HERA leads to prominent jets in the final state (see Fig. 3) and allows perturbative QCD to be applicable. The processes contributing up to first order in the strong

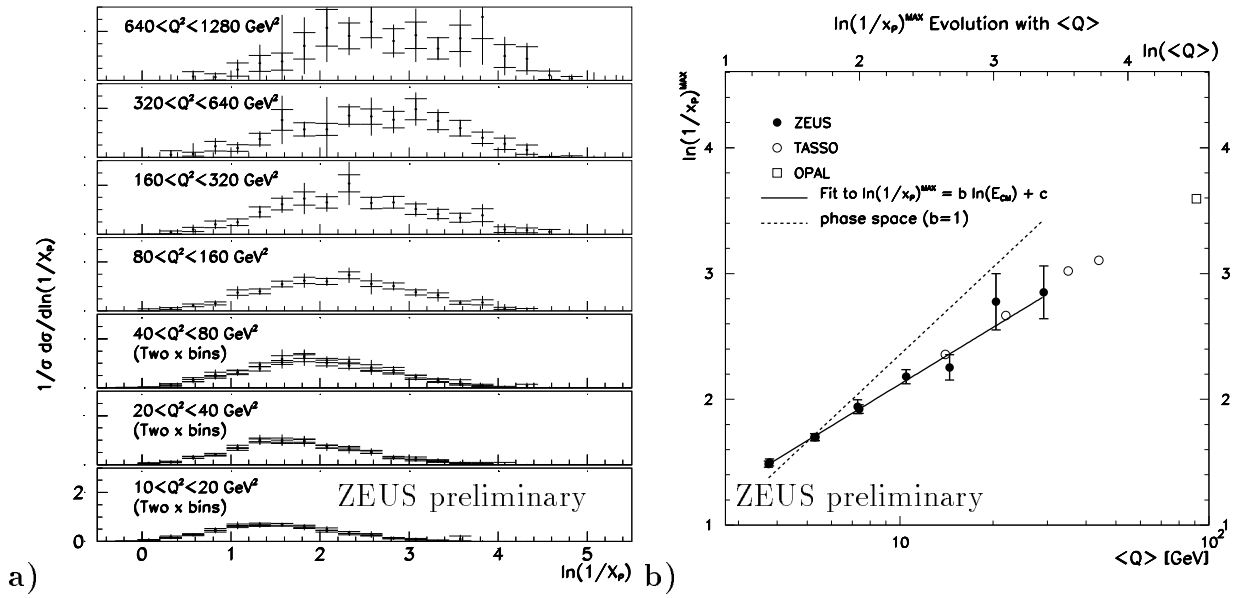

Figure 6: **a)** Charged particle spectra $\ln(1/x_p)$ with $x_p = 2p/Q$ in the Breit current region from ZEUS. Soft particles are towards the right. The inner error bars are statistical only. **a)** Peak position of the "hump backed" $\ln 1/x_p$ distributions as a function of Q . The ZEUS data (statistical errors only) are compared with data from e^+e^- annihilation

.

coupling constant α_s (Fig. 2) are the pure QPM process without gluon radiation, the QCD Compton (QCDC) process with gluon radiation in the initial or the final state, and the boson-gluon fusion process (BGF), where the photon merges with a gluon in the proton to form a quark-antiquark state. The QPM process results in a so-called "1+1" jet topology, while the QCDC and BGF processes give "2+1" jet events, where the "+1" refers to the remnant jet which escapes detection in the beam pipe.

The physics addressed so far are jet rates and the determination of α_s , and the determination of the gluon density in the proton from the rate of BGF events. Of course these two are correlated, because the production rate of 2+1 events depends on both α_s and the gluon density. At present, for large $x_{\rm part}$ one takes the gluon density function $g(x_g, Q^2)$ from parametrizations based upon structure function measurements and determines α_s , while one fixes α_s in order to measure the not yet well known gluon density at small $x_{\rm part}$. Here $x_{\rm part}$ is the momentum fraction of the parton in the proton, which equals Bjorken x only in the case when the final state produced in the hard subprocess is massless, i.e. the QPM graph.

Jets are defined, both in theory and in experiment, by a specific algorithm, which hinges upon a resolution parameter. Whether a configuration of two final state partons is called a one or a two jet configuration depends on the algorithm (e.g. JADE, cone, ...), and on the resolution parameter (inv. mass cut-off $y_{\rm cut}$, cone radius, ...). As an illustration the commonly used JADE algorithm [20] will be explained. To start with, a pseudo particle for the unobserved remnant (the "+1") is introduced in DIS. Then all particles i, j with $m_{ij}^2 < y_{\rm cut} \cdot W^2$ are merged into new particles, until no further merging is possible and the jets are reconstructed.

Apart from detector effects, the main difficulty is to correlate the observed jets with the original hard partons, which are calculable. A 1+1 configuration up to $O(\alpha_s)$ can easily turn into 2+1 after parton showers have evolved and hadronization has taken place. Experimentalists rely heavily on Monte Carlo simulations to study these effects and to invent cuts to reduce model dependencies.

Clear jet structures become visible with for example the JADE algorithm applied in the HERA laboratory frame. In Fig. 7a jet profiles from ZEUS are shown, i.e. energy flows around the found jet axis for 1+1 and 2+1 jet events. The jets become cleaner with increasing x and Q^2 , and therefore ZEUS restricts its further jet analysis to an event sample with $Q^2 > 160$ GeV^2 and $x > 0.01$, where jets are easier to detect experimentally and theoretical uncertainties are reduced. The jet profiles for this sample are well described by the MEPS and the CDM models, justifying their use for correcting the observed jet rates back to the parton level.

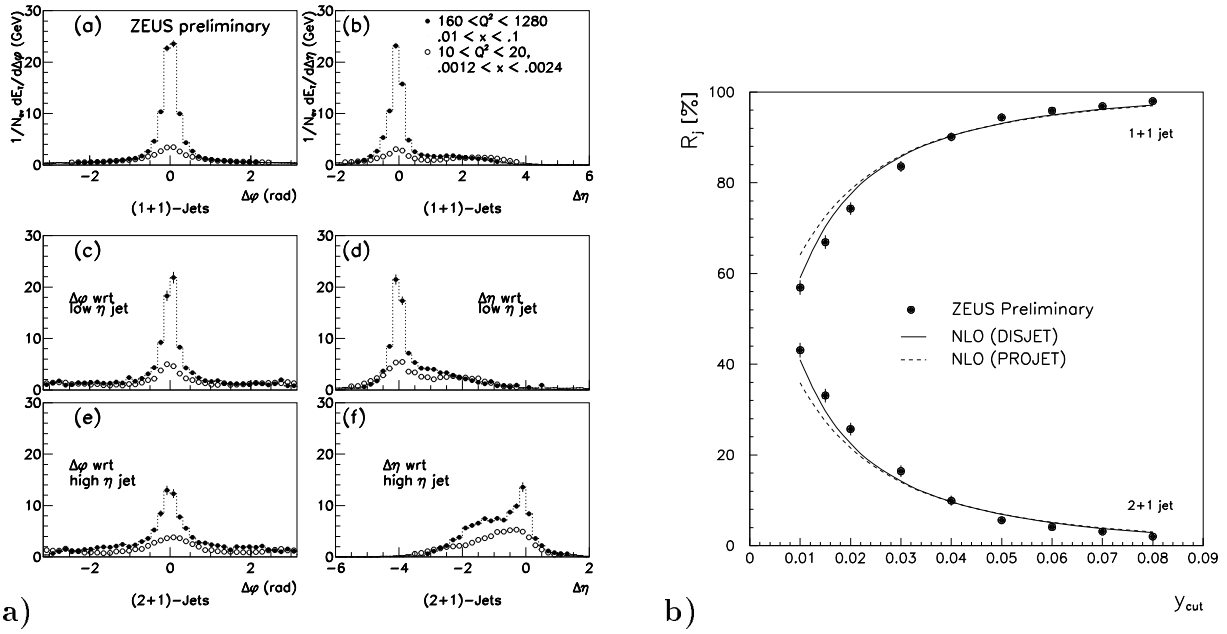

Figure 7: **a)** Jet profiles from ZEUS for 1+1 and 2+1 jet events. Plotted is the energy flow transverse to the beam axis around the jet axis in azimuth ϕ and pseudorapidity $\eta = -\ln\tan\theta/2$, where θ is the angle of the energy deposition with respect to the proton beam axis. The distance in pseudorapidity $\Delta\eta$ is measured such that the proton direction is towards the right. Shown are data from a high and a low Q^2 sample. **b)** The 1+1 and 2+1 jet rates R_j from ZEUS as a function of $y_{\rm cut}$. Calculations up to next to leading order from the programs DISJET (Brodkorb and Mirkes) and PROJET (Graudenz) for fixed $\Lambda_{\overline{\rm MS}} = 0.312$ GeV are compared to the measurements.

The rate of 2+1 jet events, normalized to the number of events which are either 1+1 or 2+1 ($R_j = N_{j+1}/(N_{1+1} + N_{2+1})$, as a function of $y_{\rm cut}$ from ZEUS is given in Fig. 7 b. Note that the data points for different values of $y_{\rm cut}$ are highly correlated. With decreasing jet resolution parameter $y_{\rm cut}$, more and more 1+1 jet events are resolved into 2+1 jet events. For a standard $y_{\rm cut}$ of 0.02 around 20% of the events are of type 2+1. Calculations up to next to leading order in α_s [21, 22] agree with the ZEUS data. It is now possible in principle to extract a value for α_s , but systematic effects and alternative analysis methods are still under study. For example the exclusion of jets close to the remnant could reduce some uncertainties from initial state parton showers.

In the H1 analysis data down to rather low Q^2 , 30 GeV^2 $< Q^2 <$ 4000 GeV^2 are included. The JADE algorithm with $y_{\rm cut}$ =0.02 is used in the HERA laboratory frame. A cut requiring $\theta_{\rm jet} > 10°$, with θ measured with respect to the proton beam axis, reduces uncertainties due to initial state parton showers. The sensitivity to the poorly known parton densities at small x is reduced by requiring $x_{\rm part} > 0.01$. For $y_{\rm cut} = 0.02$ only the 1+1 jet events are affected, because $x_{\rm part} = y_{12} + x(1 - y_{12})$, where y_{12} is the value of $y_{\rm cut}$ at which the event would turn

from 1+1 to 2+1. H1 defines the jet rates as $R_{j+1} = N_{j+1}/N_{\rm tot}$. In Fig. 8a the 2+1 jet rate is shown as a function of Q^2 , together with theoretical calculations [22] for different values of $\Lambda_{\overline{\rm MS}}$. The jet rates yield a measurement for α_s for each of the three Q^2 values (Fig. 8b). The running of α_s according to the renormalization group equation is preferred by the data.

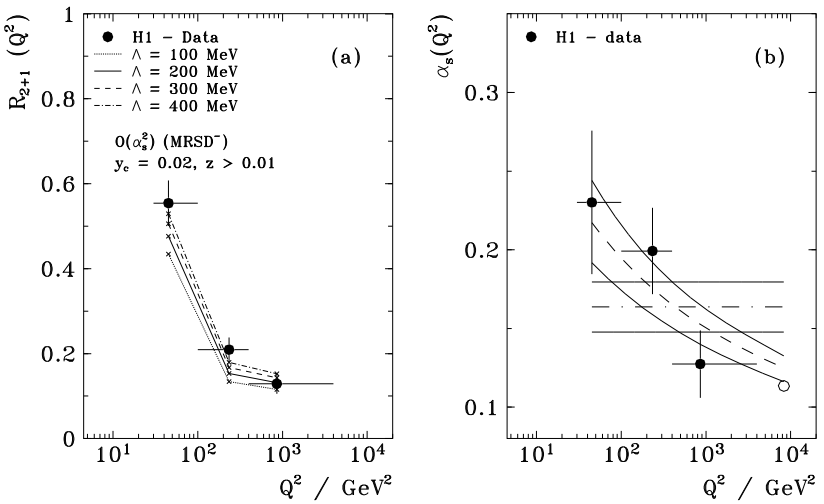

a) b)

Figure 8: **a)** The 2+1 jet rate from H1 as a function of Q^2 . Overlayed are calculations using the PROJET program with the MRSD$^-$ structure function for different values of $\Lambda_{\overline{\rm MS}}$. **b)** Measured values of α_s as a function of Q^2 . Overlayed is the best fit to the data using a running α_s , and a fit with α_s =const, together with the $\pm 1\sigma$ bands. Point to point systematic errors are not shown.

From a QCD fit to the data, α_s run to the Z mass can be obtained. The preliminary result $\alpha_s\ (M_Z^2) = 0.121 \pm 0.009({\rm stat.}) \pm 0.012({\rm syst.})$ is very promising and compares well with the value obtained at LEP [23], $\alpha_s\ (M_Z^2) = 0.119 \pm 0.003 \pm 0.010$. Considering the increase of statistics in 1994, HERA measurements of α_s will soon become competitive in precision. However, this analysis so far relies solely upon the MEPS model for corrections - systematic cross checks with other models are mandatory.

The rate of the gluon initiated BGF events provides in principle a direct measurement of the gluon density in the proton. BGF events here are operationally defined as events with large invariant masses $m_{ij} > 10$ GeV for the final state partons of the hard subprocess. This distinguishes them from sea-quark interactions, where one parton from the quark-antiquark pair does not take part in the hard scattering and stays with the remnant. The momentum fraction of the proton carried by the gluon $x_g = x_{\rm part}$ is not equal x and has to be derived from the invariant mass of the outgoing quark-antiquark pair, $x_g = (1+m^2_{q\bar{q}}/Q^2\ )\cdot x$. Experimentally it requires separating in the hadronic final state the hard subprocess from initial state parton showers and the proton remnant.

The H1 analysis is based upon an event sample at rather low Q^2 , 12.5 GeV^2 $< Q^2 <$ 80 GeV^2 and $0.035 < y < 0.625$, where the 2+1 jet rate, defined by a cone algorithm in the hadronic CMS, is dominated by BGF events. As usual, $y = Q^2\ /(x \cdot s)$. The contribution from QCDC processes, about 20 %, is subtracted statistically. The H1 result for the leading order gluon density, $x_g\ \cdot g(x_g\ , Q^2\ )$ as a function of x_g , is shown in Fig. 9 and compared with leading order parametrizations (GRV [24] and CTEQ [25]). The biggest sources of systematic errors are the dependence on the jet algorithm employed and on the QCD model used for correction.

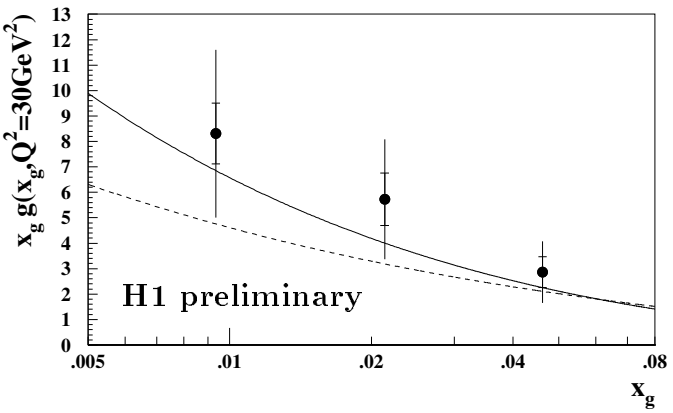

Figure 9: H1 data on the momentum weighted leading order (LO) gluon density in the proton, $x_g \cdot g(x_g, Q^2)$ as a function of x_g, compared to LO GRV (solid) and LO CTEQ 2pL (dashed) parametrizations.

5 New QCD Dynamics: Forward Jets and Energy Flows

Parton densities are conventionally evolved in Q^2 according to the GLAP (Gribov-Lipatov-Altarelli-Parisi) equations [3], starting from known input distributions in x at fixed Q^2 . Terms of order $\alpha_s \ln(Q^2/Q^2_0)$ are resummed, and terms of order $\alpha_s \ln(1/x)$ are neglected. DIS data for $x \gtrsim 10^{-2}$ are successfully described by the GLAP evolution. In the HERA small x regime however, reaching down to $x \approx 10^{-4}$, the GLAP evolution may not be applicable, because $\alpha_s \ln(1/x) \approx 1$ already at $x = 10^{-2}$ for low Q^2 . Alternatively, the BFKL (Balitsky-Fadin-Kuraev-Lipatov) equations [4] employ an evolution in x, resumming terms of order $\alpha_s \ln(1/x)$ and neglecting $\alpha_s \ln(Q^2/Q^2_0)$ terms. Consequences of this type of behaviour have not yet been seen in experiments, and it would be extremely interesting to test QCD in such a new domain. Measurements of the structure function F_2 impose constraints on the parton distributions, and at HERA, F_2 is seen to rise with decreasing x [26, 1] in accord with expectations from the BFKL equations. However, such a behaviour could also be mimicked by conventional GLAP dynamics, for a discussion of this point see [27].

More direct searches for BFKL dynamics look into the hadronic final state - remembering it contains the materialized QCD fluctuations inside the proton. The idea becomes clear from Fig. 10, depicting the evolution of partons before the hard interaction. While in GLAP the cascade is evolved in Q^2 and leads to strongly ordered parton momenta $k_{T\,j}$ transverse to the proton direction, there is no k_T ordering in BFKL, but rather in x_j, the longitudinal parton momentum scaled by the proton momentum. So far two different "footprints" of BFKL dynamics have been looked for: exclusively with "forward jets", and inclusively with energy flows. Jets with $k_{T\,\mathrm{jet}}^2 \approx Q^2$ leave little room in the cascade for a GLAP evolution, and requiring in addition $x_{\mathrm{jet}} = E_{\mathrm{jet}}/E_p \gg x$ opens a large phase space for BFKL evolution. Thus the expected rates for events with such "forward jets" should be enhanced according to the BFKL ansatz [28]. The experimental problem here is the detection of the forward jets close to the beam pipe. The second approach measures inclusively the flow of transverse energy away from the current jet. In BFKL an enhancement over GLAP expectations is expected due to the lack of strong k_T ordering; successive gluons perform a kind of random walk in k_T space.

H1 defines forward jet events by requiring $x < 2{\cdot}10^{-3}$, $x_{\mathrm{jet}} > 5{\cdot}10^{-2}$ and $0.5 < k_{T\,\mathrm{jet}}^2/Q^2 < 6$. There are more such events found than expected from the MEPS model (see Table 1)

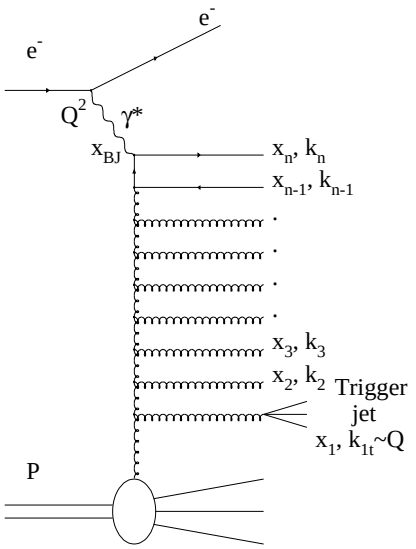

	GLAP	BFKL
evolution	in Q^2	in x
parton ordering in x	$x_1 > x_2 > ...x_j > ...x$	$x_1 \gg x_2 \gg ...x_j \gg ...x$
parton ordering in k_T	$Q_0^2 \ll k_T{}_1^2 \ll ...k_T{}_j^2 \ll ...Q^2$	"random walk" in k_T

Figure 10: Evolution of the initial state parton cascade. The characteristics for GLAP and BFKL dynamics are given in the table.

x	observed	expected (MEPS)	BFKL calc.	GLAP calc.
0.0002 - 0.001	85	37	75	25
0.0010 - 0.002	43	32	36	20

Table 1: Number of forward jets (uncorrected for acceptances) observed and expected for the data sample of 330 nb^{-1} . Also given are calculated event rates based either upon BFKL or GLAP dynamics.

which is considered to be a rather sound and complete DIS Monte Carlo based upon the GLAP equations. The excess is larger at smaller x, which is particularly intriguing as a calculation based upon the BFKL equations [29] predicts precisely the same at the parton level, in contrast to a GLAP based calculation, see Table 1. However, considering the limited statistics and various systematic effects which are still under study it is too early to draw any firm conclusions.

The flow of transverse energy E_T as a function of pseudorapidity $\eta = -\ln\tan(\theta/2)$, where θ is the angle of the energy deposition with respect to the proton beam axis, has been measured by H1 [10] at modest $Q^2 < 100$ GeV^2 for two different x bins [3], see Fig. 11 a and b.

At low x a peak from the current jet is detected more backward than at larger x , the shift being due to the event kinematics. Between the current fragmentation region and the

[3]For this analysis events with a visible "rapidity gap" [30], i.e. a region void of energy between the beam pipe and the current jet are removed (about 5% of the sample). They are presumed to stem from diffractive-like processes [2] not yet included in the standard QCD Monte Carlos.

proton remnant, a plateau of $\langle E_T \rangle \approx 2$ GeV /unit pseudorapidity is observed. Among all the models available, only CDM provides a satisfactory description of the data. Also the ZEUS data are adequately described by the CDM [31]. The model predictions are generated with the structure function parametrization MRSD$^-$ [32], which is close to the HERA F_2 measurements. In particular the MEPS model, which is based on GLAP dynamics and has been very successful in describing QCD effects at previous experiments, fails badly to describe the energy flow, mostly at low x and away from the current jet ("forward energy crisis"). It is argued that the colour dipole prescription is emulating BFKL behaviour to some extent [33], and that it at least constitutes an upper bound for any kind of BFKL like emissions [34].

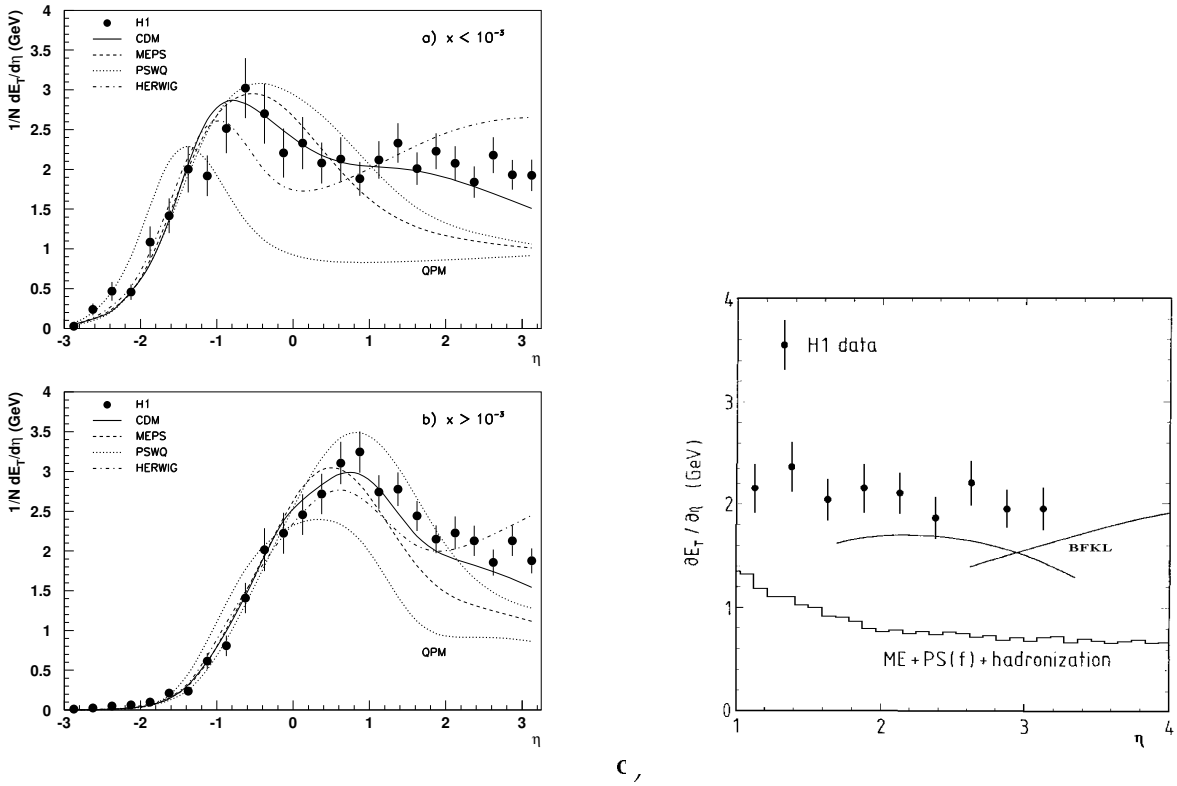

Figure 11: Transverse energy flows from H1: E_T in the laboratory system as a function of the pseudorapidity η for events with **a)** $x < 10^{-3}$ and **b)** $x > 10^{-3}$. The proton direction is to the right. An overall 6% energy scale uncertainty is not included in the error bars. **c)** Transverse energy flow calculated in the BFKL scheme, compared with the H1 low x data shown in Fig. **a)**, at $\langle x \rangle = 5.7 \cdot 10^{-4}$ and $\langle Q^2 \rangle = 15$ GeV^2 . The GLAP calculation yields ≈ 0.6 GeV in the region covered by the data. The histogram indicates the additional contribution from hadronization according to the MEPS model.

Recently, calculations of the E_T flow for HERA have become available [35, 36]. They predict a transverse energy flow per unit of pseudorapidity away from the current jet of about 2 GeV, and much less, about 0.6 GeV in the case of GLAP dynamics. The BFKL calculation is compared to the H1 data in Fig. 11c (from [36]). Unfortunately, the non-perturbative effects from hadronization are not included in the calculation. As an estimate, the contribution to the E_T flow from hadronization is shown for the MEPS model. It is not clear whether this contribution can just be added to the calculation, and it is also model dependent. For example, CDM predicts a smaller E_T contribution from hadronization. Nevertheless, the BFKL expectation is much closer to the data than the GLAP expectation - the first sign for the break down of the conventional GLAP dynamics. Whether or not this can really be explained with BFKL dynamics requires more detailed studies, for example of the x dependence of the E_T flow.

6 Conclusions

Charged particle spectra for the DIS current region at HERA tie in with precision e^+e^-data and with previous DIS data. A rich field of QCD effects in charged particle spectra has opened up and waits to be explored. It will be particularly exciting to extend the present studies further towards the target fragmentation region. First attempts to measure α_s from jet rates look very promising. The systematics are not yet completely understood, but from a statistics point of view HERA measurements will soon become competitive. Measurements of the rate of gluon induced processes have led to the first direct determination of the gluon density in the proton. The hunt for signs of new QCD dynamics, the famous "Lipatov" behaviour, in the hadronic final state has begun. The evidence from "forward jet" rates is still lacking statistics, but the study of inclusive energy flows has revealed the first sign for the breakdown of conventional Altarelli-Parisi dynamics at small x .

Acknowledgements. It is a pleasure to thank my colleagues from the ZEUS and H1 Collaborations for their help in preparing this contribution and making their preliminary results available to me.

References

[1] J. Engelen, VIth Rencontre de Blois, "Au Cœur de la Matière", Blois, June 1994.

[2] J. Bartels, VIth Rencontre de Blois, "Au Cœur de la Matière", Blois, June 1994.

[3] V.N. Gribov and L.N. Lipatov, Sov. J. Nucl. Phys. 15 (1972) 438 and 675;
G. Altarelli and G. Parisi, Nucl. Phys. 126 (1977) 297.

[4] E.A. Kuraev, L.N. Lipatov and V.S. Fadin, Sov. Phys. JETP 45 (1972) 199;
Y.Y. Balitsky and L.N. Lipatov, Sov. J. Nucl. Phys. 28 (1978) 282.

[5] H1 Collab., I. Abt et al., DESY preprint 93-103 (1993);
ZEUS Collab., M. Derrick et al., Phys. Lett. B 293 (1992) 465.

[6] S. Bentvelsen, J. Engelen, P. Kooijman, Proc. HERA workshop, Eds. W. Buchmüller and G. Ingelman, Hamburg (1991) Vol. 1, p. 23;
C. Hoeger, ibid., p. 43.

[7] G. Ingelman, Proc. HERA workshop, Eds. W. Buchmüller and G. Ingelman, Hamburg (1991) Vol. 3, p. 1366.

[8] G. Marchesini, B.R. Webber, G. Abbiendi, I.G. Knowles, M.H. Seymour and L. Stanco, Computer Phys. Comm. 67 (1992) 465.

[9] B. Andersson, G. Gustafson, L. Lönnblad and U. Pettersson, Z. Phys. C43 (1989) 625;
L. Lönnblad, Computer Phys. Comm. 71 (1992) 15.

[10] H1 Collab., I. Abt et al., Z. Phys. C94 (1994) 377.

[11] EMC Collab., M. Arneodo et al., Z. Phys. C35 (1987) 417.

[12] DELPHI Collab., P. Abreu et al., Phys. Lett. B311 (1993) 408.

[13] TASSO Collab., W. Braunschweig et al. , Z. Phys. C 45 (1989) 193;
PLUTO Collab., ibid.;
OPAL Collab., P.D. Acton et al., Z. Phys. C53 (1992) 539.

[14] Z. Koba, H.B. Nielsen and P. Olesen, Nucl. Phys. B40 (1972) 317.

[15] A.H. Mueller, Phys. Lett. B104 (1981) 161;
A. Bassetto , M. Ciafaloni, G. Marchesini and A.H. Mueller, Nucl. Phys. B207 (1982) 189;
B.I. Ermolaev and V.S. Fadin, JETP Lett. 33 (1981) 269;
Yu. L. Dokshitzer, V.S. Fadin and V.A. Khoze, Phys. Lett. B115 (1982) 242.

[16] Yu. Dokshitzer, V. Khoze, A. Mueller and S. I. Troyan, Basics of Perturbative QCD (Editions Frontière 1991).

[17] Ya. I. Azimov, Yu.L. Dokshitzer, V.A. Khoze and S.I. Troyan, Z. Phys. C27 (1985) 65.

[18] OPAL Collab., M. Z. Akrawy et al., Phys. Lett. B247 (1990) 617;
TASSO Collab., W. Braunschweig et al., Z. Phys. C47 (1990) 198.

[19] E.R. Boudinov, P.V. Chliapnikov and V.A. Uvanrov, Phys. Lett. B309 (1993) 210.

[20] JADE Collab., W. Bartel et al., Z. Phys. C33 (1986) 23.

[21] T. Brodkorb and J.G. Körner, Z. Phys. C54 (1992) 519;
T. Brodkorb and E. Mirkes, Wisconsin preprint MAD/PH/821.

[22] D. Graudenz, Phys. Lett. B256, (1991) 518 and preprint LBL-34147 (1993);
D. Graudenz, CERN preprint CERN-TH.7420/94.

[23] S. Bethke and J.E. Pilcher, Ann. Rev. of Nucl. and Particle Science 42 (1992) 251.

[24] M. Glück, E. Reya, A. Vogt, Z. Phys. C53 (1992) 127.

[25] J. Botts et al., Phys. Lett. B304 (1993) 159.

[26] H1 Collab., I. Abt et al., Nucl. Phys. B407 (1993) 515;
ZEUS Collab., M. Derrick et al., Phys. Lett. B316 (1993) 412.

[27] A. D. Martin, in Proc. of the Workshop on HERA, J. Phys. G19 (1993) 1603.

[28] A. H. Mueller, in Proc. of the Workshop on HERA, J. Phys. G19 (1993) 1463.

[29] A. D. Martin, J. Kwieciński and P. J. Sutton, Nucl. Phys. B (Proc. Suppl.) 29A (1992) 67.

[30] ZEUS Collab., M. Derrick et al., Phys. Lett. B315 (1993) 481;
H1 Collab., T. Ahmed et al., DESY preprint 94-133 (1994).

[31] ZEUS Collab., M. Derrick et al., DESY preprint 94-117 (1994).

[32] A.D. Martin, W.J. Stirling, R.G. Roberts, Phys. Lett. 306B (1993) 145.

[33] L. Lönnblad, preprint CERN-TH.7307/94 (1994);
A. H. Mueller, Nucl. Phys. B415 (1994) 373.

[34] B. Andersson, private communication.

[35] J. Kwieciński, A.D. Martin, P.J. Sutton and K.Golec-Biernat, Phys. Rev. D50 (1994) 217.

[36] J. Kwieciński, A.D. Martin, P.J. Sutton and K.Golec-Biernat, Durham preprint DTP/94/30.